HHS Public Access

Author manuscript

Neuron. Author manuscript; available in PMC 2018 January 02.

Published in final edited form as:

Neuron. 2016 November 23; 92(4): 888–901. doi:10.1016/j.neuron.2016.09.059.

A mechanosensory circuit that mixes opponent channels to produce selectivity for complex stimulus features

Allison E. B. Chang[1], **Alex G. Vaughan**[2,3], and **Rachel I. Wilson**[1,*]

[1]Department of Neurobiology, Harvard Medical School, Boston, MA 02115

[2]Janelia Research Campus, Howard Hughes Medical Institute, Ashburn, VA 20147

Abstract

Johnston's organ is the largest mechanosensory organ in *Drosophila*; it analyzes movements of the antenna due to sound, wind, gravity, and touch. Different Johnston's organ neurons (JONs) encode distinct stimulus features. Certain JONs respond in a sustained manner to steady displacements, and these JONs subdivide into opponent populations that prefer push or pull displacements. Here, we describe neurons in the brain (aPN3 neurons) that combine excitation and inhibition from push/pull JONs in different ratios. Consequently, different aPN3 neurons are sensitive to movement in different parts of the antenna's range, at different frequencies, or at different amplitude modulation rates. We use a model to show how the tuning of aPN3 neurons can arise from rectification and temporal filtering in JONs, followed by mixing of JON signals in different proportions. These results illustrate how several canonical neural circuit components – rectification, opponency, and filtering – can combine to produce selectivity for complex stimulus features.

Introduction

All sensory systems face the problem of encoding signals over a broad dynamic range. A common strategy is to divide signals into a pair of opponent channels. For example, in the vertebrate and fly retina, some cells encode luminance increases while others encode decreases (Behnia and Desplan, 2015; Masland, 2012). In the vertebrate auditory brainstem, some cells respond to sound intensity increases while others respond to decreases (Joris et al., 2004). Similarly, in the fish electrosensory system, some cells encode increases in electric fields while others encode decreases (Clarke et al., 2015). This sort of arrangement raises some basic questions. Do opponent channels ultimately converge again? If so, does the split have any consequences for neural codes downstream of the convergence?

*Lead Contact: rachel_wilson@hms.harvard.edu.

[3]Present address: Cold Spring Harbor Laboratory, Cold Spring Harbor, NY 11724

Author contributions: A.E.B.C. performed the experiments, analyzed the data, and implemented the modeling. A.E.B.C. and R.I.W. designed the experiments and wrote the manuscript. A.G.V. shared the *70G01-Gal4* line prior to its original publication.

Johnston's organ, the largest mechanosensory organ in *Drosophila*, provides an interesting example of opponent coding. It resides in the antenna and consists of >400 mechanosensory neurons (Kamikouchi, 2013; Murthy, 2010). It encodes movements of the distal antennal segment elicited by sound, wind, touch, or other forces. Some JONs are steadily depolarized by a sustained displacement that pushes the antenna toward the head ("push JONs"), whereas others are steadily depolarized by a sustained displacement away from the head ("pull JONs"; Figure 1A; Kamikouchi et al., 2009; Matsuo et al., 2014; Yorozu et al., 2009). As JONs project into the brain, the axons of push and pull JONs segregate into different branches. Push JONs dominate the "E" branch, whereas pull JONs dominate the "C" and "D" branches (Matsuo et al., 2014; Yorozu et al., 2009).

Push and pull JONs have mainly been studied in the context of sustained antennal displacements (Kamikouchi et al., 2009; Matsuo et al., 2014; Yorozu et al., 2009). However, these same JONs can also respond to sound (Figure S1; Mamiya and Dickinson, 2015). Whereas other JON types are fast enough to track individual sound cycles (Eberl et al., 2000; Lehnert et al., 2013), there is no evidence that push/pull JONs are this fast; rather, they seem to only encode the slow component of the sound stimulus – i.e., the envelope of sound amplitude modulations (Figure 1B). In this regard, it is notable that push and pull JONs divide up the antenna's range of movement, meaning that they encode a rectified version of the antenna's position (Kamikouchi et al., 2009; Matsuo et al., 2014; Yorozu et al., 2009). In abstract terms, rectifying a waveform before low-pass filtering is a standard way to extract the amplitude modulation envelope of the waveform. This may be what enables push/pull JONs to respond to sound amplitude modulations (Figure 1C).

In short, push and pull JONs are interesting because they represent opponent channels. They are also interesting because they seem to encode both sustained displacements and the amplitude modulation envelope of antennal vibrations. However, almost nothing is known about how the brain processes signals from push/pull JONs. Investigating these circuits in the brain may offer the opportunity to study how opponent channels converge, and how specific features of modulation envelopes are extracted.

In this study, we describe neurons in the brain (aPN3 neurons) that combine excitation from push JONs with inhibition driven by both push and pull channels. Collectively, aPN3 neurons encode the low-frequency components of antennal movement (DC to 50 Hz), including steady deflections, sound amplitude modulations, and slow features of wind-like stimuli. Notably, different aPN3 neurons combine push and pull inputs in different ratios. As a consequence, they exhibit diverse selectivity for specific spatiotemporal stimulus features. We build a model to show how the response properties of these neurons can arise from rectification and temporal filtering in JONs, followed by linear mixing of opponent JON signals in variable proportions. Our findings illustrate how seemingly complex response properties can emerge from basic circuit components – rectification, opponency, and filtering. Because these components are common to many systems, including visual, auditory, and electrosensory systems (Baker, 1999; Clarke et al., 2015), our findings have general significance for how circuits can implement a wide range of signal-processing tasks.

Results

aPN3 neurons receive input from C/E JONs, but not A/B JONs

The dendrites of aPN3 neurons reside in the brain region targeted by JON axons (Figure S2) and are reported to overlap with the E branch of the JON axon bundle (Matsuo et al., 2016; Vaughan et al., 2014). We began by reexamining the overlap between JON axons and aPN3 neuron dendrites. We used specific Gal4 lines to label the C/E branches of the JON axon bundle with one protein marker and the aPN3 neurons with another marker. We found that the aPN3 dendrites were completely confined to the region defined by C/E JONs (Figure 1D). There is no Gal4 line specific to the E bundle in particular, but as both C and E branches are dominated by push and/or pull JONs, it is clear that aPN3 dendrites overlap with push and/or pull JON axons. We also confirmed that aPN3 dendrites do not overlap with the “A” or “B” branches of the JON axon bundle (Figure 1E). The A and B branches contain fast JONs that encode individual sound cycles and do not respond in a sustained manner to steady displacements (Lehnert et al., 2013; Matsuo et al., 2014; Yorozu et al., 2009).

Next, we tested for functional connectivity between JONs and aPN3 neurons. We expressed CsChrimson in JONs that innervate the C/E branches. We then performed GFP-targeted *in vivo* whole-cell current clamp recordings from aPN3 neurons while transiently illuminating the antenna. We found that stimulating the C/E JONs evoked a mixture of excitation and inhibition (Figure 1F). Excitation typically preceded inhibition, which suggests a direct excitatory input from the E and possibly also C JON axon branches, as well as an indirect inhibitory input via interposed inhibitory interneurons in this brain region (Matsuo et al., 2016). Interestingly, excitation dominated some aPN3 neurons, whereas inhibition dominated others. In still other neurons, excitation and inhibition were nearly balanced. When we bath-applied antagonists of synaptic inhibition, excitation always grew larger. In the cells that were net inhibited by the stimulus, blocking synaptic inhibition revealed underlying excitation (Figure 1F). Together, these results imply that each aPN3 neuron receives both excitation and inhibition driven by the E and/or C branches of the JON axon bundle, but the ratio of these inputs varies across neurons. Similar results were obtained with a different Gal4 line that drives expression in the C/E branches (Figures S3 and S4). We also repeated this experiment using a specific driver for JONs that innervate the A/B branches and found no evidence for input from these JONs (Figure S4).

Finally, we confirmed that JONs in the C/E branches were sufficient to confer normal stimulus-evoked responses on aPN3 neurons. In a fly harboring a mutation in the *iav* gene that renders JONs silent (Gong et al., 2004; Lehnert et al., 2013), we rescued *iav* in the C/E axon branches alone. Stimulus-evoked responses in these flies were indistinguishable from wild type responses (Figure S5), indicating that the C/E JONs are sufficient to confer normal responsiveness on the aPN3 neurons.

In short, these experiments indicate that aPN3 neurons receive input from JONs in the E and/or C branch, but not the A or B branch. This input consists of both excitation and inhibition. Finally, different aPN3 neurons combine excitation and inhibition in different ratios.

Diversity in responses to sustained displacements

To begin to characterize aPN3 neuron tuning, we used a piezoelectric actuator to push and pull on the antenna (Figure 2A). To ensure that the antenna was rotating as it does normally, we visualized the antenna and the probe using two video cameras placed at different angles. We began by using static deflections of the antennae because these stimuli are known to drive robust opponent responses in push and pull JONs. Static deflections are also behaviorally relevant to flies; they can indicate the presence of a steady wind, orientation with respect to gravity, or the presence of foreign material on the antennae. Indeed, push/pull JONs contribute to behavioral responses to many of these stimuli (Hampel et al., 2015; Kamikouchi et al., 2009; Yorozu et al., 2009).

We found that most aPN3 neurons were depolarized by pushing the antenna toward the head (positive displacements; Figure 2A). Conversely, they were hyperpolarized by pulling the antenna away from the head (negative displacements). Depolarization and hyperpolarization were accompanied by increases and decreases in spike rate. Responses generally adapted over several seconds (Figure 2A; mean τ was 1.1 sec/5.2 sec for 1-μm push/pull steps). Adaptation was typically incomplete, meaning that there was a tonic response at steady state. Slow JON responses also adapt modestly (Yorozu et al., 2009), and so adaptation in aPN3 neurons may be at least partly inherited from their JON inputs.

As a group, aPN3 neurons encoded push and pull stimuli in a graded manner, as reflected in the mean membrane potential (Figure 2B) and spike rate (Figure 2C) of the entire population. We can take the slope of the displacement-response curve (Δ voltage / Δ displacement) as a measure of a cell's sensitivity (Figure 2D). In individual neurons, sensitivity to push and pull could be asymmetric (Figure 2E). Some neurons were more sensitive to push, while others were more sensitive to pull. In short, there was substantial diversity among aPN3 neurons in the part of the antenna's dynamic range where sensitivity was maximal.

Push and pull inputs to aPN3 neurons

Given the diverse response profiles of different aPN3 neurons, we hypothesized that these neurons receive different mixtures of synaptic inputs. Our optogenetic experiments indicate that the balance of excitation and inhibition varies across the aPN3 population (Figure 1F). Excitation and inhibition could arise from either push JONs or pull JONs, or both (Figure 3A). It is important to keep in mind that push and pull JONs respond bidirectionally: movements in the preferred direction evoke strong depolarization, and movements in the null direction evoke weak hyperpolarization (Figure 1A; Kamikouchi et al., 2009; Matsuo et al., 2014; Yorozu et al., 2009). Thus, any given antennal movement could elicit responses in all four potential input channels (push+, push−, pull+, pull−).

To deduce the contribution of synaptic inhibition to aPN3 responses, we bath-applied antagonists of inhibitory neurotransmitter receptors (picrotoxin and CGP54626). In some neurons, the antagonists disinhibited the excitatory response to pushing (Figures 3B and 3C). We can therefore infer that in these neurons, pushing recruits not only increased excitation (push+), but also increased inhibition (push−).

In other neurons, depolarizing responses to pushing were actually reduced by the antagonists (Figures 3B and Figure 3C). This could occur if pull JONs drove tonic inhibitory input (pull −) onto these neurons. Pushing would withdraw this tonic inhibition, leading to depolarization.

Thus, because the antagonists had opposing effects in different neurons, the ratio of push−/pull− input is likely to vary across the aPN3 neuron population. This result also suggests that the depolarization evoked by push stimuli is driven by both increased excitation from push JONs and decreased inhibition from pull JONs, with the ratio of these two inputs varying across cells.

What about pulling stimuli? In most neurons, the antagonists reduced or eliminated hyperpolarization evoked by pulling (Figures 3B and 3C), implying that pulling recruits synaptic inhibition (pull−). However, in some neurons, some residual hyperpolarization remained, likely reflecting withdrawal of tonic excitatory input from push JONs (push+). In a few cells, the antagonists reversed the hyperpolarizing response to pulling so that it became depolarizing (Figures 3B and 3C). This would imply that these cells receive excitation from pull JONs (pull+), although this seems to be the weakest or least common of the four inputs to the aPN3 population. Together, these results suggest that the hyperpolarization evoked by pull stimuli is driven by both increased inhibition from pull JONs and decreased excitation from push JONs, again with these two inputs varying across cells.

In summary, we can understand the effect of the antagonists in each cell as arising from a particular mixture of excitation and inhibition driven by opponent JON inputs (Figure 3D). Overall, the average effect of the antagonists was statistically significant for pull stimuli but not push stimuli (Figure 3C). However, this is a situation where the interesting result resides not in the average effect, but in the nature of the cell-to-cell variation.

In principle, bath application of these antagonists could produce indirect effects due to network disinhibition. Therefore, we also tried injecting positive current through the recording electrode to hold these neurons at a depolarized potential. This manipulation should decrease the driving force for excitation and increase the driving force for inhibition. In most cells, we found this decreased the depolarizing response to pushing (Figures 3E and 3F). This is what we would expect if pushing recruits mainly an increase in excitation (push +), with or without and increase in inhibition (push−). If pushing recruited mainly disinhibition in most cells (via a withdrawal of inhibition from the pull− channel), then we would expect the opposite result (Figure 3G).

When we injected positive current into the recording electrode, we saw a larger hyperpolarizing response to pulling in some cells (Figures 3E and 3F). This is what we would expect if pulling recruits mainly an increase in inhibition (pull−). In other cells, however, there was almost no net change in the hyperpolarizing response to pulling, which is what we would expect if pulling recruits both an increase in inhibition (pull−) and a decrease in excitation (via a withdrawal of the push+ channel; Figure 3G).

In short, these data support the hypothesis that different aPN3 neurons receive different mixtures of synaptic inputs. Excitation from push JONs (push+) appears to be the dominant input overall. Inhibition from both opponent channels also plays a major role (push− and pull−). The weakest input overall appears to be excitation from pull JONs (pull+).

Excitatory and inhibitory inputs to aPN3 neurons have different dynamics

In the course of these experiments, we noticed that inhibition was more transient than excitation. For example, pushing elicited sustained depolarization in most aPN3 neurons, but in some cases this response was interrupted by a hyperpolarizing “notch” near the onset of the step. This notch disappeared when synaptic inhibition was blocked (e.g., Figure 3B, top row). Moreover, this notch became larger when the cell was held at a depolarized potential (e.g., Figure 3E, all example cells). Thus, the notch represents inhibition that is more transient than excitation.

Hyperpolarizing responses to pulling also appeared to have a transient component in many cells (e.g., Figure 3B, bottom row), and this was generally eliminated by blocking synaptic inhibition. Transient hyperpolarizing responses to pulling were also magnified by holding the cell at a depolarized potential (e.g., Figure 3E, middle row). Again, these observations suggest that pulling evokes inhibition that is more transient than excitation.

Together, these results indicate that the inhibitory inputs to these neurons (push− and pull−) have a prominent transient component, whereas the excitatory inputs (push+ and pull+) are more sustained. We have seen that the balance of excitation and inhibition differs across aPN3 neurons. Because inhibition and excitation have different dynamics, the dynamics of the net response should therefore also vary across aPN3 neurons. This helps to explain why a given stimulus elicits different dynamics in different neurons (Figure 3B and 3E). As we will see, the difference between the dynamics of excitation and inhibition will become important to explain certain features of the aPN3 neuron population.

Sound excites some aPN3 neurons and inhibits others

Next, we investigated how aPN3 neurons respond to sound. Because slow JONs encode the amplitude modulation envelope of a sound (Mamiya and Dickinson, 2015), we might expect aPN3 neurons to do the same. We began by using a sound stimulus consisting of a 200 Hz tone. This frequency is near the antenna’s resonance frequency for low-intensity sounds (Gopfert and Robert, 2002). It is also the dominant frequency of *Drosophila* wingbeats in flight (Lehmann and Dickinson, 1997) and of courtship song (Murthy, 2010). We modulated this tone at 4 Hz.

We found that most aPN3 neurons phase-locked to the 4-Hz amplitude modulation envelope of this sound stimulus (Figure 4A). Interestingly, some neurons were depolarized by each sound pip, whereas others were hyperpolarized. We call these ON and OFF cells, respectively.

The distinction between ON and OFF aPN3 cells was also evident in their spiking. ON cells fired at pip onset, whereas OFF neurons fired at pip offset. OFF cells spiked at pip offset because hyperpolarization offset elicits an intrinsic rebound depolarization in most aPN3

neurons (data not shown). In response to a periodic train of sound pips, ON and OFF cells spiked at different phases (Figure 4B). However, when synaptic inhibition was blocked, all neurons fired in phase with the stimulus (Figures 4A and 4B).

In short, sounds elicited anticorrelated responses in aPN3 neurons, whereas static displacements elicited correlated responses (Figure 2). A static displacement is a low-frequency stimulus (a DC stimulus). We therefore hypothesized that low-frequency stimuli should elicit strongly correlated responses across the aPN3 population, and only high-frequency stimuli should elicit anticorrelated responses. As predicted, when we used the piezoelectric actuator to impose a low-frequency vibration on the antenna (a 1 Hz oscillation), we found that aPN3 neurons responded in a correlated fashion, with all neurons firing spikes roughly in phase with each other (Figures 4C and 4D). However, vibrations at 25 Hz or above caused ON and OFF responses to emerge (Figure 4C), yielding spikes at a variety of phases (Figure 4D). Thus, the ON/OFF distinction was prominent when the stimulus contained high frequencies, but it disappeared when the stimulus contained only low frequencies.

A model of aPN3 neuron responses

It is clear that the aPN3 population can respond robustly to a wide range of stimuli. Interestingly, a given pair of cells can be either correlated or anti-correlated, depending on the stimulus. Here, we develop a simple model to explain how this can arise based on the main synaptic inputs we have already inferred – i.e., excitation from push JONs combined with inhibition driven by both push and pull JONs. (To make our model's behavior more easily understandable, we omit the fourth input: excitation from pull JONs. Including this input does not change our qualitative conclusions, and it also helps our model generate better fits.)

The JON portion of the model is based on published data (Figure 5A, left). JON responses grow sigmoidally with antennal displacement (Effertz et al., 2012; Effertz et al., 2011; Kamikouchi et al., 2009; Lehnert et al., 2013; Yorozu et al., 2009). In push/pull JONs, responses are rectified (Kamikouchi et al., 2009; Matsuo et al., 2014; Yorozu et al., 2009), meaning the antenna's resting position should be below the mid-point of the sigmoid. The responses of push/pull JONs to step displacements resemble smoothed versions of the stimulus, and the model captures this with a low-pass filter. Finally, the responses of push/pull JONs adapt over several seconds (Yorozu et al., 2009). In fast JONs, adaptation can be explained by a horizontal shift of the curve in the direction of the stimulus (Lehnert et al., 2013), and the same sort of adaptation occurs in vertebrate hair cells (Corey and Hudspeth, 1983), so we model adaption in this manner for push/pull JONs as well (dashed curves in Figure 5A).

Model push and pull Jons track the sound envelope in a correlated manner (Figure 5B). However, they respond to static displacements in an opponent manner (Figure 5B).

Our model envisions that aPN3 neurons simply sum excitation from push JONs (push+) with inhibition driven by push and pull JONs (push− and pull−). The push+ and pull− inputs should be correlated in response to static displacements, but anti-correlated in response to

sound pips (Figure 5C). Thus, a pair of aPN3 neurons that combined these two inputs in very different ratios would generate coherent responses to static displacements, but opponent responses to sound (Figure 5D). This is just what we observe in our data: aPN3 neurons respond in a coherent manner to static displacements (Figure 2), but they break into ON and OFF populations in response to sound (Figure 4).

What happens when we add inhibition driven by push JONs (push−)? With a static displacement stimulus, push− antagonizes both push+ and pull−. With a sound stimulus, the situation is different: push− reinforces pull− but antagonizes push+ (Figure 5C). Thus, by combining these three inputs in different ratios, we can vary the relative magnitude of responses to static displacements and sounds.

We have so far passed over a feature of the model that requires explanation. Recall that inhibition is more transient than excitation (Figure 3). In order to capture this, we passed the two inhibitory inputs through a bandpass filter (Figure 5A). The properties of the bandpass filter were tuned to match our aPN3 neuron data. This feature of the model is not directly relevant to the phenomenon of frequency-specific opponency (which is our focus in this section), but we include it in the model because it will become important in fitting other features of aPN3 neuron responses (see below).

A simple model captures responses to static displacements and vibrations

We next asked whether this model could qualitatively account for the wide diversity of aPN3 neuron responses. We recorded from a large number of aPN3 neurons, employing a piezoelectric actuator attached to the antenna to create both static displacements and vibrations. We then fit the model to these cells. The only free parameters in the model were the weights on the three input channels (push+, pull−, push−).

The model was able to capture all of the major features of the data, as well as much of the diversity we observed in the aPN3 neuron population (Figures 6A and 6B). For example, we could generate model cells with variable sensitivity to positive versus negative static displacements. We could also capture the fact that the magnitude of the sound response varied relative to the static displacement response.

Importantly, the fitted weights (Figure 6B) were consistent with our experiments dissecting the inputs to aPN3 neurons. Every model neuron received a push+ input. Most received a pull− input, and most received a push− input. For most model neurons, the push+ input was stronger than the push− input.

In the remainder of this study, we will illustrate how different aPN3 neurons extract diverse spatiotemporal features of sensory stimuli. We will use the model to show how this diversity can be captured by simply varying the weights of the three main inputs to these neurons. This circuit architecture allows aPN3 neurons to tile a large stimulus space along multiple stimulus dimensions.

Diverse temporal selectivity: envelope frequency tuning

One relevant stimulus dimension is the frequency of sound amplitude modulation (the "envelope" modulation frequency; Figure 7A). Different aPN3 neurons responded preferentially to different envelope frequencies (Figure 7B). In general, neurons that were bandpass-tuned to envelope frequency were OFF neurons (i.e., they were hyperpolarized by each sound pip). Conversely, neurons that were low-pass tuned were ON neurons (i.e., they were depolarized by each sound pip). After synaptic inhibition was blocked, bandpass tuning was lost, and all cells displayed low-pass tuning (Figure 7B). These findings provide further support for our conclusion that excitatory inputs are low-pass filtered, whereas inhibitory inputs are bandpass filtered, and it is the difference between the kinetic properties of these inputs that accounts for some of the temporal tuning of aPN3 neurons.

Our model could reproduce the envelope tuning properties of real aPN3 neurons. Some model neurons we fitted to the data in Figure 6 were low-pass tuned to envelope frequency, whereas others were bandpass tuned (Figure 7C). Just as in the data, the bandpass neurons were the OFF neurons, whereas the low-pass neurons were the ON neurons. When we zeroed all the inhibitory weights in these model neurons (mimicking the effect of blocking synaptic inhibition), they all assumed low-pass characteristics, again like real aPN3 neurons (Figure 7C). The weights in this set of model neurons were only fitted to the stimuli in Figure 6, and so it is notable that the model accurately predicts responses to these new stimuli. The model shows how, when excitation and inhibition have different frequency tuning, diversity in tuning can arise from combining excitation and inhibition in different ratios. Here, because excitation is low-pass tuned, and inhibition is a bandpass-filtered version of excitation, adding more inhibition shifts tuning toward higher frequencies.

Diverse temporal selectivity: carrier versus envelope

Another relevant stimulus dimension is the carrier vibration frequency. Although aPN3 neurons cannot phase lock to the carrier we have been using thus far (200 Hz), they can phase-lock to lower frequencies. When we varied the carrier between 15 and 50 Hz (Figure 7D), we found that virtually all neurons showed at least a small voltage oscillation at the lowest carrier frequency, and they were all low-pass tuned over this range of frequencies (Figure 7E). Some neurons showed large oscillations at the carrier frequency, and these were often ON neurons, or else neurons intermediate between ON and OFF (Figures 7F and 7G). Other cells showed much less power at the carrier frequency, and these were often OFF neurons. Overall, there was a systematic correlation between power at the carrier frequency and ON/OFF characteristics (Figure 7F).

We used our model to understand how this correlation arises. We selected representative cells, and we fit the three input weights in our model to match the responses of these cells. The OFF cells were best fit by a model with approximately equal inhibition from the two opponent channels (push− and pull−). These model OFF cells generally showed poor phase-locking to the carrier, just like real OFF cells (e.g., cell 1 and cell 2, Figure 7G). The reason is that push− and pull− are 180° out of phase at the carrier frequency (Figure 7H), so they add destructively to suppress the carrier. But push− and pull− add constructively at the envelope frequency, and so these cells show strong phase-locking to the envelope.

Conversely, model ON cells were of course dominated by push+ input. These cells generally showed better phase locking to the carrier, just like real ON cells (e.g., cell 3, Figure 7G). Because these cells are mainly driven by a single input, their frequency characteristics are simply inherited from that input, with no destructive interference.

The best carrier frequency phase-locking occurred in model cells that were dominated by a combination of push+ and pull− (e.g., cell 4, Figure 7G). The push+ and pull− inputs are approximately in phase at the carrier frequency, and so they add constructively to amplify the carrier (Figure 7H). However, they are out of phase at the envelope frequency, and so they add destructively to suppress the envelope. Thus, the model helps explain why there is a general tradeoff between carrier and envelope.

Diverse temporal selectivity: tuning to wind-evoked movements

Finally, we considered wind stimuli. Wind contains power over a broad range of frequencies, and in this respect it differs from the narrowband vibration stimuli we have used until now (i.e., pure tones). We began by using laser Doppler vibrometry to measure antennal movements evoked by a gentle turbulent air flow. We then created a random sequence of artificially-induced antennal movements that emulated the broadband spectral properties of this wind-evoked movement. We used a piezoelectric actuator to impose this movement on the antenna while recording from aPN3 neurons.

We found that different aPN3 neurons reliably spiked at different moments during the fictive wind stimulus, indicating that they responded selectively to different features of this stimulus (Figure 8A). Model aPN3 neurons displayed the same general phenomenon (Figure 8B). Notably, the weights in this set of model neurons were only fitted to the stimuli in Figure 6 (static displacements and amplitude-modulated sounds), and yet the model accurately captures the nature of diverse responses to fictive wind stimuli as well. This is further evidence that the mechanisms that produce temporal diversity among aPN3 neurons allow the population to transmit information about a relatively broad range of temporal features, including the broadband features of wind stimuli.

Discussion

Our experimental results indicate that aPN3 neurons combine excitation driven mainly by push JONs with inhibition driven by both push and pull JONs. Our model explains how, by combining these inputs in different ratios, aPN3 neurons can achieve diverse tuning with respect to several different stimulus features. Specifically, different aPN3 neurons are (1) sensitive over different parts of the antenna’s dynamic range, (2) tuned to different amplitude modulation frequencies, and (3) differentially phase-locked to either first-order modulations (carrier) or second-order modulations (envelope). Thus, in response to a wide range of stimuli, different aPN3 neurons respond at different levels or at different times. In general terms, our results show how splitting a signal into opponent channels, and then recombining those two channels downstream, can affect the format of neural codes downstream from the point of recombination. The key point is that mixing opponent channels in different ratios can create a range of tuning properties, with different mixtures exploiting different aspects of the way that opponent channels are rectified and filtered.

Diverse sensitivity to movement in different parts of the antenna's range

We found that some aPN3 neurons are most sensitive in the positive part of the antenna's range, while others are most sensitive in the negative part of the antenna's range (Figure 2, Figure 6). Our model shows this can arise because push JONs are most sensitive in the positive part of the antenna's range, whereas pull JONs are most sensitive in the negative part (Figure 5A; Kamikouchi et al., 2009; Matsuo et al., 2014; Yorozu et al., 2009). By combining push and pull inputs in variable ratios, aPN3 neurons can achieve sensitivity over different parts of this range.

Moreover, in different parts of the antenna's range, different aPN3 neurons are more or less sensitive to vibration amplitude modulations. A fly standing on an incline facing downward will have its antennae displaced away from the head (Kamikouchi et al., 2009). We found that this positional bias conferred better sensitivity to vibration amplitude modulations on some neurons, but poorer sensitivity on other neurons (Figure S6). Our model explains how this can occur. If the antennae are biased away from the head, this puts a vibrating stimulus into the more linear part of the pull JON curve, meaning that the responses of pull JONs are less rectified, and therefore are more strongly attenuated by subsequent low-pass filtering. Pull and push channels can add either constructively or destructively in different aPN3 neurons, so sensitivity to vibrations may either increase or decrease (Figure S6).

Interestingly, an analogous phenomenon occurs in the retina. Here, luminance is the first-order stimulus (analogous to antennal position in our case), and contrast is the second-order stimulus (analogous to antennal vibration amplitude in our case). In the retina, a luminance bias can change the amount of rectification in the synaptic inputs to a retinal ganglion cell, and thereby change its sensitivity to contrast (Grimes et al., 2014). Our results conceptually extend this idea by showing how a first-order bias (position, luminance, etc.) can have different effects on second-order sensitivity (contrast sensitivity, vibration amplitude sensitivity) depending on the mix of opponent channels that provide input to each neuron.

Diverse tuning to amplitude modulation frequency

Amplitude modulations (i.e., envelope modulations, or second-order modulations) are a feature of all sensory stimuli. For example, sound amplitude modulations (AM) is a key factor in determining the intelligibility of speech (Elliott and Theunissen, 2009). In the visual system, AM signals can be used to distinguish objects based on their contrast or texture and to detect object motion (Chubb et al., 2001). It is therefore of general interest to learn how neural circuits can extract features of AM signals.

We found that different aPN3 neurons are tuned to different AM frequencies (Figure 7). ON neurons tended to prefer lower AM frequencies, whereas OFF neurons tended to prefer higher AM frequencies. When synaptic inhibition was blocked, all neurons shifted to preferring low AM frequencies. A mechanistic explanation for this phenomenon is that inhibition is more transient than excitation. In experiments using step displacement stimuli (Figure 3), we often observed a transient component of step-evoked hyperpolarization that was blocked by antagonists of inhibitory neurotransmitter receptors. Our model shows that if

inhibition is more transient than excitation, then neurons that combine inhibition and excitation in different ratios will prefer different AM frequencies.

Our results have a precedent in studies of the vertebrate auditory system, where much of the selectivity for sound amplitude modulation frequency begins in the brainstem. *In vivo* intracellular recordings are challenging in the brainstem, and so the cellular mechanisms underlying AM frequency tuning are not fully understood (Joris et al., 2004). Some evidence supports one mechanism that involves the interaction of excitatory and inhibitory inputs that have different latencies. Cells that receive different amounts of inhibition display different AM tuning, and AM responses are strongest when excitation and inhibition are maximally out of phase (Grothe, 1994; Yang and Pollak, 1997). Here we extend these results by illustrating the consequence of a mismatch of a different sort – namely, a mismatch in the frequency tuning of excitation and inhibition (low-pass versus bandpass). We show how, given this sort of mismatch, AM selectivity can be tuned by varying the balance of excitation and inhibition, without any explicit lag in the arrival of inhibition.

Mechanisms of AM encoding in the visual system are also not fully understood, but there appear to be both retinal and cortical contributions (Demb et al., 2001; Orger et al., 2000). In particular, there is evidence that cortical neurons combine spatially mismatched excitation and inhibition arising from rectified-and-filtered input channels (Hallum and Movshon, 2014). Our results suggest that it would be interesting to compare the frequency characteristics of these inputs.

Diverse mixtures of first- and second-order stimulus encoding

We found that different aPN3 neurons encode either the first-order stimulus (the carrier vibration) or the second-order stimulus (the envelope), or both (Figure 7). Our model shows how this phenomenon can arise. The key point is that push and pull JONs respond in an anti-correlated manner to the first-order stimulus (Yorozu et al., 2009), but they respond in a positively-correlated manner to the second-order stimulus (Mamiya and Dickinson, 2015). Thus, model neurons dominated by a roughly equal mixture of inhibition driven by the two opponent channels (push− and pull−) show little response to the carrier frequency but strong responses at the amplitude modulation frequency. Meanwhile, the opposite is true of neurons dominated by a mixture of feedforward excitation and opponent inhibition (push+ and pull −); they display little power at the amplitude modulation frequency but sizeable power at the carrier frequency, provided that the carrier is slow enough (< 50 Hz).

Interestingly, a similar phenomenon occurs in the fish electrosensory system (Clarke et al., 2015; McGillivray et al., 2012). Here, two types of excitatory pyramidal cells have anti-correlated responses to lower-order modulations in the electric field, but they have positively correlated responses to higher-order modulations. Neurons that are postsynaptic to these pyramidal cells encode only the lower-order stimulus or the higher-order stimulus, depending on whether they receive input from one cell type or both.

This phenomenon also occurs in the retina. Some retinal ganglion cells combine excitation from one opponent channel with inhibition driven by another opponent channel. These two synaptic inputs produce positively correlated changes in the postsynaptic cell with regard to

the first-order stimulus feature (luminance), but because they are rectified and then low-pass filtered, they produce anti-correlated effects with regard to the second-order stimulus feature (contrast). As a consequence, postsynaptic cells that integrate these inputs can encode the first-order stimulus while truncating their responses to the second-order stimulus (Cafaro and Rieke, 2013; Molnar et al., 2009; Werblin, 2010).

Simplifications and generalizations of our model

Throughout this study, we have relied on a model to understand aPN3 neuron responses. The model is constrained by the data we obtained in this study on the circuit inputs to aPN3 neurons, together with published data on the properties of push and pull JONs. The major result of this model is that the diversity of aPN3 responses can be largely explained by linear mixing of these three inputs in different ratios.

The model is obviously a simplified view of this system. The model contains just one rectifying step (at the level of JONs), one low-pass filter (at the level of JONs), and one bandpass filter (at the level of inhibitory inputs). In reality, there may be multiple rectifying and filtering steps in this system – at the stage of JON spike generation, synaptic transmission, and aPN3 synaptic integration. Our model likely lumps many biological processes into a minimal set of operations. Also, the model contains only two model JONs with identical dynamics and identical (mirror-image) sensitivity. However, there may be more diversity in the JON inputs to these cells.

The goal of the model was to show how seemingly complicated phenomena can arise from known properties of JONs, along with circuit elements that are directly supported by our data. The simplicity of our model makes it easier to understand how these elements interact, and it also makes the model's significance more general: the same model could stand as a hypothesis about how rectified and filtered opponent channels might be combined in other sensory circuits. These circuit elements are common building blocks, and so it is not surprising that aPN3 neurons have some functional similarities with neurons in the vertebrate retina, the vertebrate auditory system, and the fish electrosensory system (Baker, 1999; Clarke et al., 2015; Joris et al., 2004). Our results highlight the fact that simply combining these circuit elements in variable ratios can yield diverse selectivity along multiple dimensions of time and space.

Experimental Procedures

Genotypes

Figure 1D: *JO31-Gal4/ey-FLP;70G01-Gal4,UAS-CD2/UAS-FRT-stop-FRT-CD8:GFP*

Figure 1E: *70G01-LexA/13xLexAop2-CD8:GFP;JO15-Gal4/UAS-CD2*

Figure 1F: *JO31-Gal4/20XUAS-IVS-CsChrimson.mVenus;10xUAS-IVS-CD8:GFP/ 10xUAS-IVS-CD8:GFP,70G01-Gal4*

Figures 2–8: *10xUAS-IVS-CD8:GFP,70G01-Gal4*

Genotypes used in supplemental figures are noted in the corresponding figure legends. See Supplemental Experimental Procedures for details on transgenic lines.

Electrophysiology

Whole-cell patch-clamp recordings were performed *in vivo* from GFP-labeled aPN3 neuron somata in currentclamp mode. The brain was continuously perfused with oxygenated saline. The small amplitude of the spikes in these neurons (~10 mV) is likely due to the spike initiation zone being some distance from the soma. For details see Supplemental Experimental Procedures.

Calcium imaging

Calcium imaging in Figure S1 was performed in vivo from GCaMP6s-expressing JON axon terminals using a two-photon excitation microscope. The preparation was the same as for the electrophysiological experiments, except that the head was rotated 180° relative to the body in order to image the ventral part of the brain, where JON axons terminate. Images were acquired near the z-level of the AP sub-bundle of the A JON axon bundle (Kamikouchi et al., 2006). For details see Supplemental Experimental Procedures.

Pharmacology

We used picrotoxin and CGP54626 to block synaptic inhibition. In *Drosophila*, picrotoxin is an antagonist of GABA-A receptors (Wilson and Laurent, 2005) and GluCl receptors (Liu and Wilson, 2013), and CGP54626 is an antagonist of GABA-B receptors (Wilson and Laurent, 2005). Drugs were bath-applied via the saline perfusate. In some experiments, CGP54626 was omitted (as indicated). For details see Supplemental Experimental Procedures.

Immunohistochemistry

Commercial antibodies were used in standard protocols. For details see Supplemental Experimental Procedures.

Piezoelectric stimulation

We used either a closed-loop piezoelectric actuator (Physik Instrumente P-841.60, 90 μm travel range, with E-509.S1 sensor/piezo servo-control module) or an open-loop piezoelectric actuator (Physik Instrumente P-840.60, 90 μm travel range, with E-505 amplifier and E-500 chassis). In the latter case, a laser Doppler vibrometer was used to measure the movement of the actuator in a separate set of calibration experiments, and the voltage commands to the actuator were adjusted in an iterative calibration procedure to achieve the desired movement trajectory. The actuator was coupled to the fly's arista via a stiff probe attached to the most distal branch point of the arista using tiny drop of adhesive. To ensure that the probe was inducing purely rotational (naturalistic) movements of the antenna, we used two video cameras placed at different angles to monitor the movement of the antenna in each experiment. For details see Supplemental Experimental Procedures.

Optogenetic stimulation

Flies were reared in cultures supplemented with all-trans retinal. To stimulate ipsilateral JONs, the second antennal segment was illuminated with a fine fiber optic filament coupled to a green LED. Because the light was focused on the antenna, and the antenna is separated from the brain by titanium foil, we would expect relatively little directly stimulation of aPN3 neurons (which also expressed CsChrimson). Moreover, the voltage command to the LED was adjusted (to approximately 0.5 μW) so that illumination of the antenna produced no more than 2 mV of direct excitation in aPN3 neurons (as assessed by washing on 1 μM TTX at the end of each experiment and measuring the magnitude of the TTX-insensitive response). For details see Supplemental Experimental Procedures.

Acoustic stimulation

Sound stimuli were delivered using a speaker ~14 cm from the fly at an angle of ~45° (relative to the fly's long axis) so that sound energy was directed at an angle perpendicular to the arista ipsilateral to the recorded aPN3 neurons. The speaker was electrically and mechanically isolated from the recording setup. Sound intensity (in units of particle velocity) at the position of the fly was measured using a calibrated particle velocity microphone. For details see Supplemental Experimental Procedures.

Laser Doppler vibrometry and fictive wind stimulus

We first used a laser Doppler vibrometer to measure the antenna's movement in response to a wind stimulus generated in the laboratory using an array of fans. The time-averaged wind speed generated by these fans was 0.4 m/s. We then used these measurements to generate controlled and repeatable stimuli with the piezoelectric actuator having similar frequency and amplitude content. Gaussian noise was filtered so that the power spectrum resembled that of wind-evoked antennal movements (most energy was below 200 Hz) and scaled so that its amplitude matched that of wind-evoked movement (standard deviation of 2.35 μm). For details see Supplemental Experimental Procedures.

Modeling, statistics, and data analysis

See Supplemental Experimental Procedures.

Supplementary Material

Refer to Web version on PubMed Central for supplementary material.

Acknowledgments

We thank Gerry Rubin, Barret Pfeiffer, and Bill Lemon for the gift of flies harboring the modified UAS-DenMark construct (*pJFRC-TLN-cherry* in attP40). We thank Craig Montell for the gift of *iav*^{1}*;;UAS-iav* flies. The screen that identified *70G01-Gal4* was performed by A.G.V when he was a student in the lab of Bruce Baker, who generously shared this reagent. We are grateful to David Corey, Katherine Nagel, Brendan Lehnert, Elizabeth Hong, Dan Polley, Rick Born, Kamal Sen, Christopher Harvey, and John Assad for advice throughout the project. Members of the Wilson Lab provided feedback on the manuscript. A.E.B.C. was supported by an NSF Graduate Research Fellowship and a Kirschstein-NRSA predoctoral fellowship (F31) award from the NIH. R.I.W. is an HHMI Investigator. Support for this work was provided by an HFSP Program Grant.

References

Baker CL Jr. Central neural mechanisms for detecting second-order motion. Curr Opin Neurobiol. 1999; 9:461–466. [PubMed: 10448168]

Behnia R, Desplan C. Visual circuits in flies: beginning to see the whole picture. Curr Opin Neurobiol. 2015; 34:125–132. [PubMed: 25881091]

Cafaro J, Rieke F. Regulation of spatial selectivity by crossover inhibition. J Neurosci. 2013; 33:6310–6320. [PubMed: 23575830]

Chubb C, Olzak L, Derrington A. Second-order processes in vision: introduction. J Opt Soc Am A Opt Image Sci Vis. 2001; 18:2175–2178. [PubMed: 11551051]

Clarke SE, Longtin A, Maler L. Contrast coding in the electrosensory system: parallels with visual computation. Nat Rev Neurosci. 2015; 16:733–744. [PubMed: 26558527]

Corey DP, Hudspeth AJ. Kinetics of the receptor current in bullfrog saccular hair cells. J Neurosci. 1983; 3:962–976. [PubMed: 6601694]

Demb JB, Zaghloul K, Sterling P. Cellular basis for the response to second-order motion cues in Y retinal ganglion cells. Neuron. 2001; 32:711–721. [PubMed: 11719210]

Eberl DF, Hardy RW, Kernan MJ. Genetically similar transduction mechanisms for touch and hearing in Drosophila. J Neurosci. 2000; 20:5981–5988. [PubMed: 10934246]

Effertz T, Nadrowski B, Piepenbrock D, Albert JT, Gopfert MC. Direct gating and mechanical integrity of Drosophila auditory transducers require TRPN1. Nat Neurosci. 2012; 15:1198–1200. [PubMed: 22842145]

Effertz T, Wiek R, Gopfert MC. NompC TRP channel is essential for Drosophila sound receptor function. Curr Biol. 2011; 21:592–597. [PubMed: 21458266]

Elliott TM, Theunissen FE. The modulation transfer function for speech intelligibility. PLoS Comput Biol. 2009; 5:e1000302. [PubMed: 19266016]

Gong Z, Son W, Chung YD, Kim J, Shin DW, McClung CA, Lee Y, Lee HW, Chang DJ, Kaang BK, et al. Two interdependent TRPV channel subunits, inactive and Nanchung, mediate hearing in Drosophila. J Neurosci. 2004; 24:9059–9066. [PubMed: 15483124]

Gopfert MC, Robert D. The mechanical basis of Drosophila audition. J Exp Biol. 2002; 205:1199–1208. [PubMed: 11948197]

Grimes WN, Schwartz GW, Rieke F. The synaptic and circuit mechanisms underlying a change in spatial encoding in the retina. Neuron. 2014; 82:460–473. [PubMed: 24742466]

Grothe B. Interaction of excitation and inhibition in processing of pure tone and amplitude-modulated stimuli in the medial superior olive of the mustached bat. J Neurophysiol. 1994; 71:706–721. [PubMed: 8176433]

Hallum LE, Movshon JA. Surround suppression supports second-order feature encoding by macaque V1 and V2 neurons. Vision Res. 2014; 104:24–35. [PubMed: 25449336]

Hampel S, Franconville R, Simpson JH, Seeds AM. A neural command circuit for grooming movement control. Elife. 2015; 4:e08758. [PubMed: 26344548]

Joris PX, Schreiner CE, Rees A. Neural processing of amplitude-modulated sounds. Physiol Rev. 2004; 84:541–577. [PubMed: 15044682]

Kamikouchi A. Auditory neuroscience in fruit flies. Neurosci Res. 2013; 76:113–118. [PubMed: 23707240]

Kamikouchi A, Inagaki HK, Effertz T, Hendrich O, Fiala A, Gopfert MC, Ito K. The neural basis of Drosophila gravity-sensing and hearing. Nature. 2009; 458:165–171. [PubMed: 19279630]

Kamikouchi A, Shimada T, Ito K. Comprehensive classification of the auditory sensory projections in the brain of the fruit fly Drosophila melanogaster. J Comp Neurol. 2006; 499:317–356. [PubMed: 16998934]

Lehmann FO, Dickinson MH. The changes in power requirements and muscle efficiency during elevated force production in the fruit fly Drosophila melanogaster. J Exp Biol. 1997; 200:1133–1143. [PubMed: 9131808]

Lehnert BP, Baker AE, Gaudry Q, Chiang AS, Wilson RI. Distinct roles of TRP channels in auditory transduction and amplification in Drosophila. Neuron. 2013; 77:115–128. [PubMed: 23312520]

Liu WW, Wilson RI. Glutamate is an inhibitory neurotransmitter in the Drosophila olfactory system. Proc Natl Acad Sci U S A. 2013; 110:10294–10299. [PubMed: 23729809]

Mamiya A, Dickinson MH. Antennal mechanosensory neurons mediate wing motor reflexes in flying Drosophila. J Neurosci. 2015; 35:7977–7991. [PubMed: 25995481]

Masland RH. The neuronal organization of the retina. Neuron. 2012; 76:266–280. [PubMed: 23083731]

Matsuo E, Seki H, Asai T, Morimoto T, Miyakawa H, Ito K, Kamikouchi A. Organization of projection neurons and local neurons of the primary auditory center in the fruit fly Drosophila melanogaster. J Comp Neurol. 2016; 524:1099–1164. [PubMed: 26762251]

Matsuo E, Yamada D, Ishikawa Y, Asai T, Ishimoto H, Kamikouchi A. Identification of novel vibration- and deflection-sensitive neuronal subgroups in Johnston's organ of the fruit fly. Front Physiol. 2014; 5:179. [PubMed: 24847281]

McGillivray P, Vonderschen K, Fortune ES, Chacron MJ. Parallel coding of first- and second-order stimulus attributes by midbrain electrosensory neurons. J Neurosci. 2012; 32:5510–5524. [PubMed: 22514313]

Molnar A, Hsueh HA, Roska B, Werblin FS. Crossover inhibition in the retina: circuitry that compensates for nonlinear rectifying synaptic transmission. J Comput Neurosci. 2009; 27:569–590. [PubMed: 19636690]

Murthy M. Unraveling the auditory system of Drosophila. Curr Opin Neurobiol. 2010; 20:281–287. [PubMed: 20362428]

Orger MB, Smear MC, Anstis SM, Baier H. Perception of Fourier and non-Fourier motion by larval zebrafish. Nat Neurosci. 2000; 3:1128–1133. [PubMed: 11036270]

Vaughan AG, Zhou C, Manoli DS, Baker BS. Neural pathways for the detection and discrimination of conspecific song in D. melanogaster. Curr Biol. 2014; 24:1039–1049. [PubMed: 24794294]

Werblin FS. Six different roles for crossover inhibition in the retina: correcting the nonlinearities of synaptic transmission. Vis Neurosci. 2010; 27:1–8. [PubMed: 20392301]

Wilson RI, Laurent G. Role of GABAergic inhibition in shaping odor-evoked spatiotemporal patterns in the Drosophila antennal lobe. J Neurosci. 2005; 25:9069–9079. [PubMed: 16207866]

Yang L, Pollak GD. Differential response properties to amplitude modulated signals in the dorsal nucleus of the lateral lemniscus of the mustache bat and the roles of GABAergic inhibition. J Neurophysiol. 1997; 77:324–340. [PubMed: 9120574]

Yorozu S, Wong A, Fischer BJ, Dankert H, Kernan MJ, Kamikouchi A, Ito K, Anderson DJ. Distinct sensory representations of wind and near-field sound in the Drosophila brain. Nature. 2009; 458:201–205. [PubMed: 19279637]

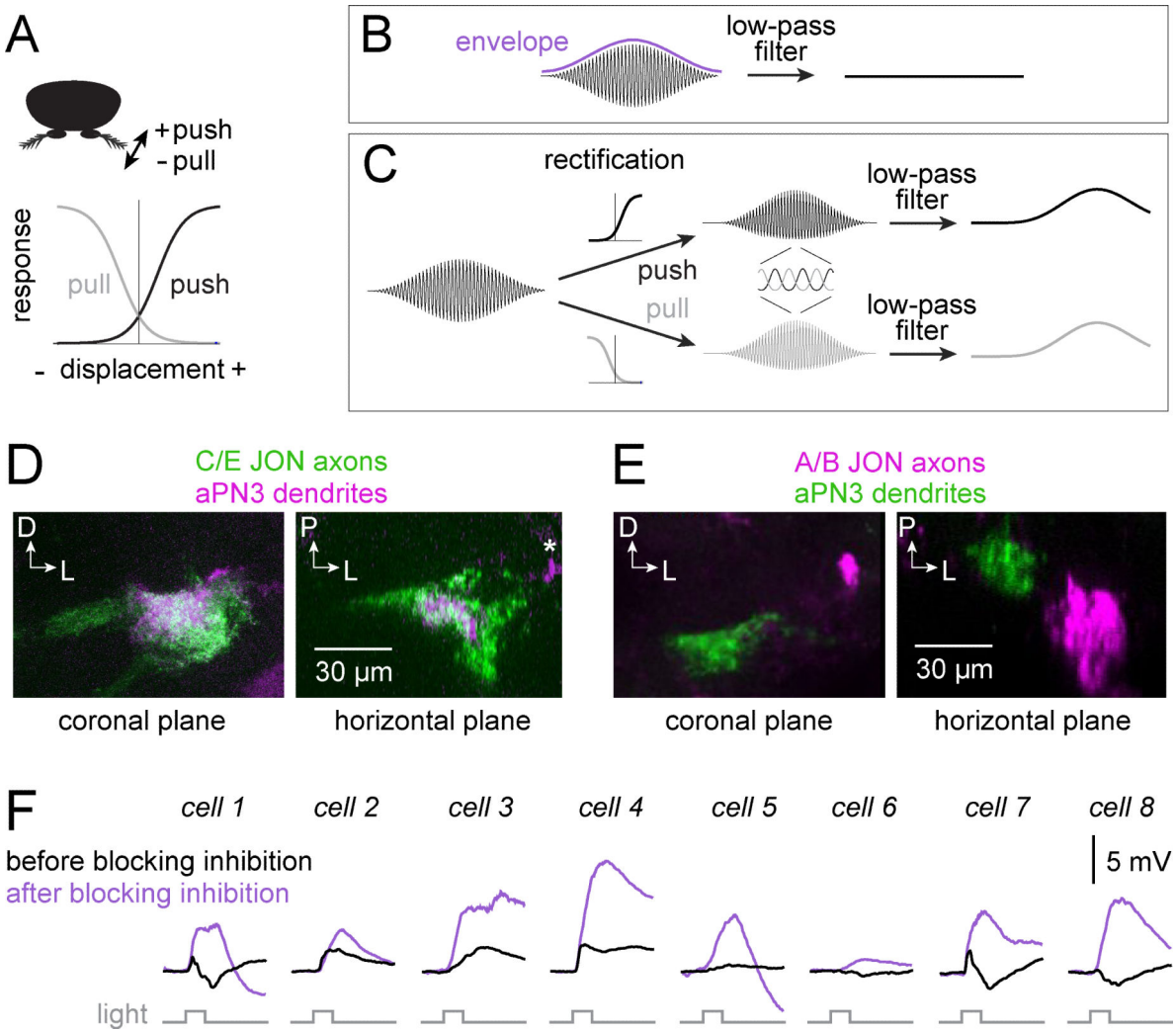

Figure 1. Push/pull JONs and their inputs to aPN3 neurons

A) Schematic of push and pull JON responses. Zero displacement (vertical line) represents the antenna's resting position.

B) Carrier and envelope components of a sound waveform. Low-pass filtering the waveform would attenuate both the carrier and the envelope.

C) Schematic showing how push and pull JONs can extract the envelope by rectifying the sound waveform before low-pass filtering it. Prior to low-pass filtering, the outputs of the two channels are anti-correlated with respect to the first-order stimulus (inset). After low-pass filtering, the outputs of the two channels are positively correlated, and they encode the envelope (the second-order stimulus).

D) Anatomical evidence for push and/or pull input to aPN3 neurons. Push JONs dominate the E branch of the JON axon bundle in the brain, whereas pull JONs dominate the C and D branches (Matsuo et al., 2014; Yorozu et al., 2009). aPN3 neurons expressing CD2 (magenta) overlap with the axons of C/E JONs expressing both CD8:GFP and CD2 (green). Both coronal and horizontal planes are shown. The aPN3 dendrites were completely enveloped by the C/E axons at all planes in the confocal z-stack, and we find no evidence

that the aPN3 dendrites extend outside the region defined by C/E axons. The lateral patch of CD2 signal in this plane (asterisk) is part of the aPN3 axonal arborization in the wedge (Figure S2).

E) aPN3 neurons expressing CD8:GFP (green) do not overlap with the axons of A/B JONs expressing CD2 (magenta).

F) aPN3 neuron responses to optogenetic stimulation of C/E JONs (light pulse is 50 msec, n=8 cells). CsChrimson is expressed under the control of the C/E driver *JO31-Gal4*. Traces represent the average voltage response (meaning spikes are clipped and the voltage is then trial-averaged; the same is true in all other cases where “average voltage” responses are shown). Blocking synaptic inhibition (with 5 μM picrotoxin and 50 μM CGP54626) revealed excitation in every cell. At the end of each experiment, we added tetrodotoxin (TTX) to the bath (2 μM) to confirm that most of the aPN3 response relied on spiking in JONs.

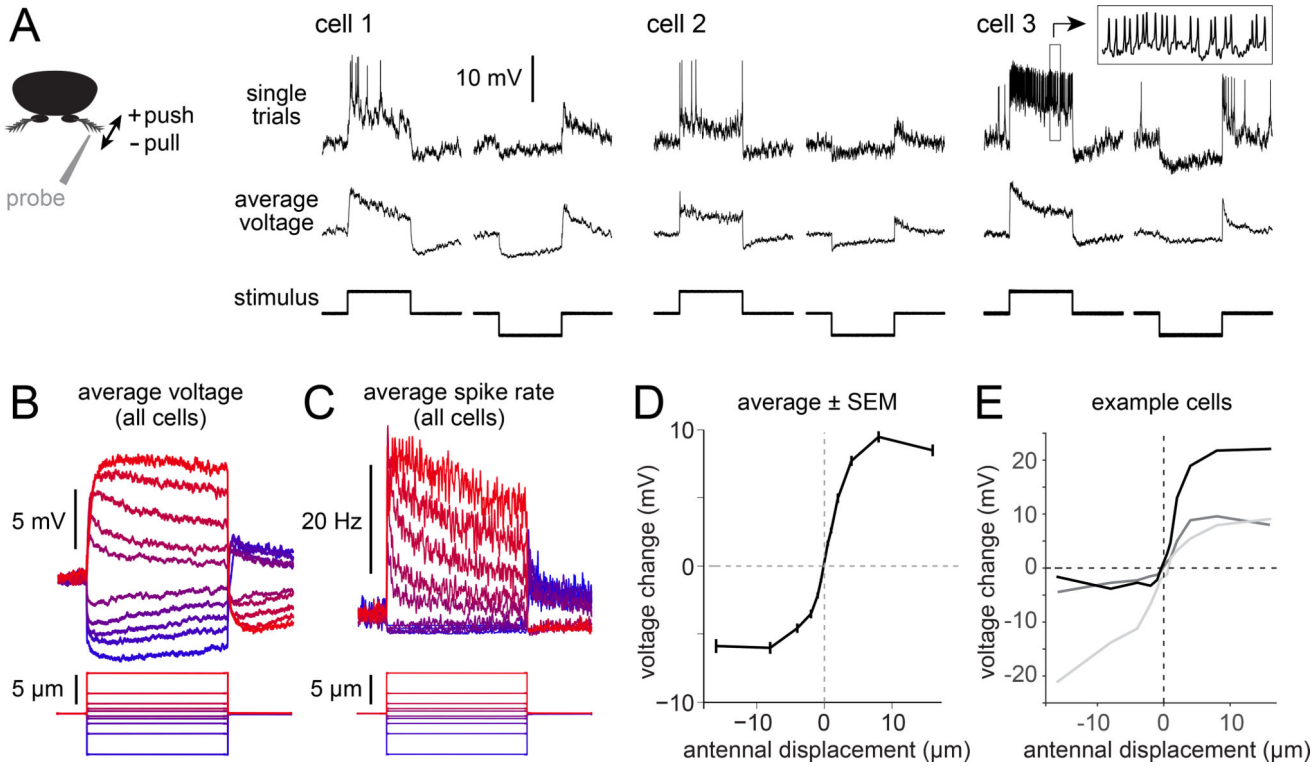

Figure 2. aPN3 neurons bidirectionally encode antennal position

A) Responses to static displacements for three example aPN3 neurons (positive = push, negative = pull). Top: single traces. Note spikes, about 10 mV in amplitude. Inset shows a snippet of spiking activity (boxed region) with the time scale expanded 15-fold. Bottom: average voltage (i.e., the trial-averaged voltage after clipping spikes). Stimuli are displacements of 2 µm, 5 sec in duration.

B) Average voltage responses to a family of displacements for the aPN3 population (±0.5, 1, 2, 4, and 8 µm, 5 sec in duration). Data are averaged across all recorded aPN3 neurons that were tested with these stimuli (n=20 cells in 14 flies).

C) Same as (B) but for spike rates. With small displacements, adaptation is visible in both the average voltage and the spike rate. With large displacements, adaptation is visible in the spike rate but not the average voltage; this may be due in part to the fact that spiking prevents the membrane potential from maintaining a sustained depolarization above the spike threshold.

D) Displacement-response curve for the aPN3 population (n=20 cells in 14 flies). The response is quantified over a window 2 – 5 sec after step onset.

E) Same as (D) but for three example cells. The slope of this function is a measure of a cell's sensitivity to movement. Some cells are most sensitive to positive movements, whereas others are most sensitive to negative movements.

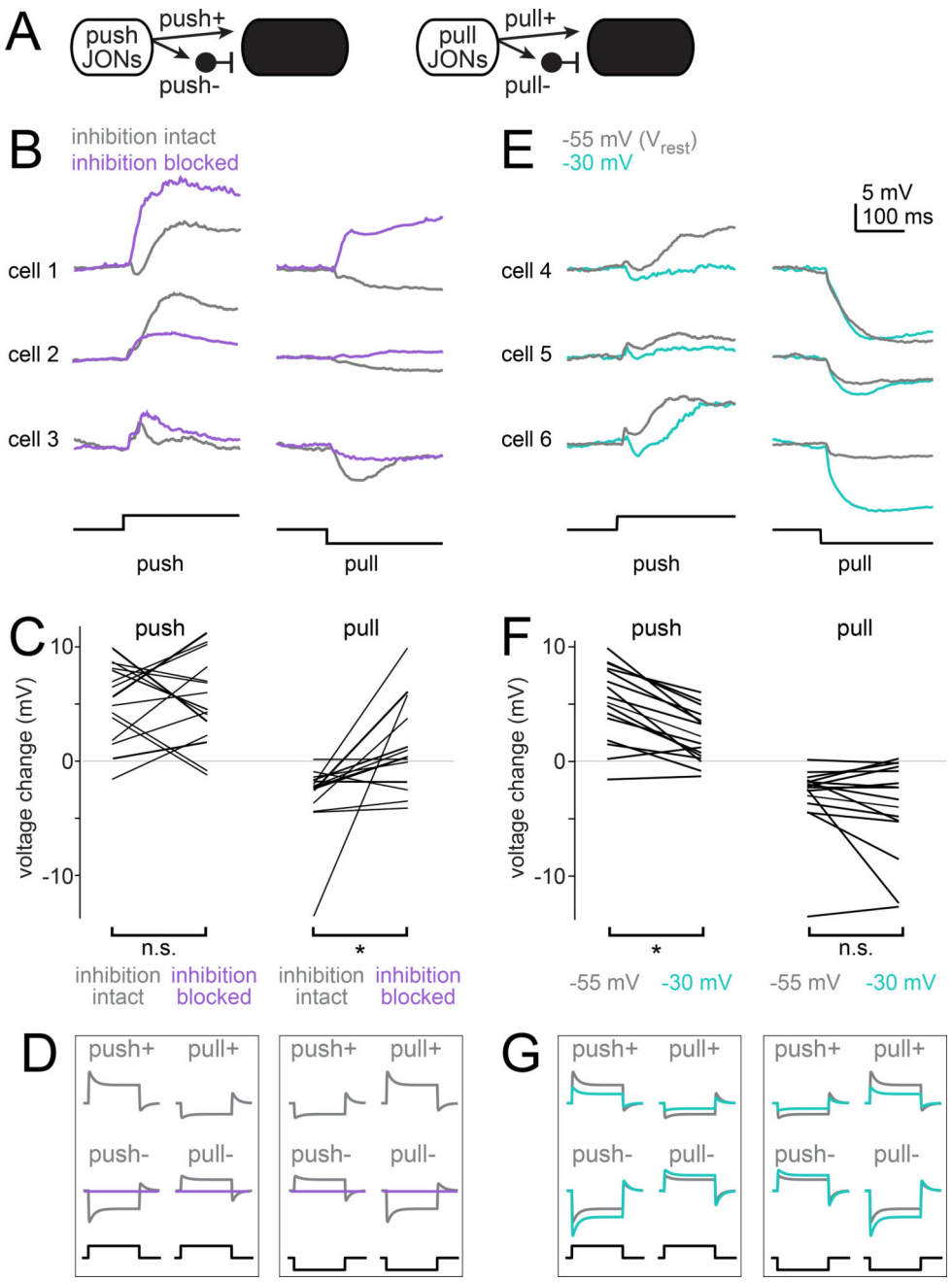

Figure 3. Identifying inputs to aPN3 neurons driven by different JON types

A) Four potential inputs to aPN3 neurons. Inhibitory inputs are schematized as arising from an interposed local neuron.

B) In three example aPN3 neurons, blocking synaptic inhibition (with 5 μM picrotoxin and 50 μM CGP54626) changes voltage responses to step displacements in diverse ways. Stimuli are deflections of 3.125 μm.

C) Sustained change in average voltage evoked by these deflections, before and after blocking synaptic inhibition (n = 15 cells in 15 flies). Responses were measured over a window 100 – 250 msec after step onset. Overall, blocking inhibition significantly

attenuated the hyperpolarizing response to pulling ($p = 0.0112$), whereas the effect for pushing was not significant because different cells showed opposing results ($p = 0.9463$). All tests in this figure are paired two-tailed t-tests.

D) Schematic of the four potential inputs to aPN3 neurons, showing predicted effects of eliminating synaptic inhibition (purple).

E) In three example aPN3 neurons, injecting positive current to depolarize the cell (thereby increasing inhibition and decreasing excitation) changes responses to step displacements in diverse ways. As before, stimuli are deflections of 3.125 μm. Traces represent average voltage at normal resting potential (~ −55 mV) and a depolarized potential (~ −30 mV).

F) Sustained change in average voltage, with and without positive current injection ($n = 15$ cells in 15 flies). Overall, this manipulation significantly attenuated the response to pushing ($p = 8 \times 10^{-5}$), whereas the effect for pulling was not significant because different cells showed opposing results ($p = 0.221$).

G) Schematic of the four potential inputs to aPN3 neurons, showing predicted effects of positive current injection (blue).

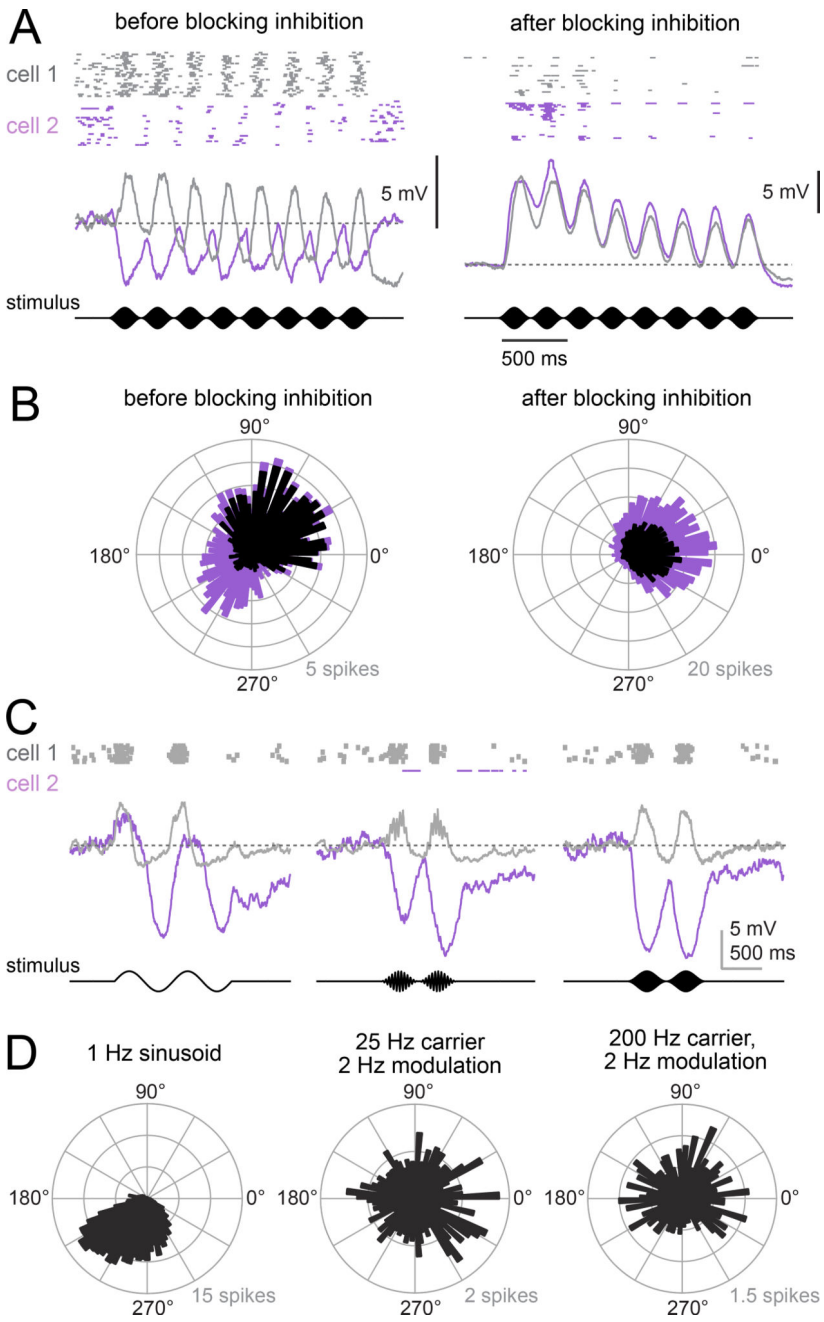

Figure 4. aPN3 neurons can be depolarized or hyperpolarized by sound

A) Responses of two example aPN3 neurons to an amplitude-modulated sound stimulus (200 Hz carrier modulated at 4 Hz, particle velocity ~ 20 mm/s). Left: before blocking inhibition, rasters and average voltage. Right: the same two cells with synaptic inhibition blocked (5 μM picrotoxin and 50 μM CGP54626). These cells are anticorrelated before blocking inhibition, but correlated after inhibition is blocked. (Note that baseline firing rates are difficult to compare because the drugs caused a tonic depolarization which we counteracted by injecting a small amount of negative current.)

B) Phase histograms of spikes in a population of aPN3 cells in response to the same stimulus (spikes per cell, n = 18 cells in 18 flies). Phase is measured as lag from the stimulus amplitude modulation envelope, with zero degrees denoting spikes occurring at the positive peak of the stimulus. Left: before blocking inhibition. Each bin is stacked with OFF cells (purple) on top of ON cells (black). On average, ON and OFF cells are about 180° out of phase. Right: with synaptic inhibition blocked (5 μM picrotoxin with or without 50 μM CGP54626). Each cell is color coded as before, although now all cells show ON behavior. C) Responses of two example cells to stimuli at various frequencies (1 Hz sinusoid, a 25 Hz carrier modulated at 2 Hz, and a 200 Hz carrier modulated at 2 Hz; ± 1.5 μm). Responses to the slow stimulus are correlated, whereas responses to the faster stimuli are anticorrelated. D) Phase histograms of spikes in a population of aPN3 cells in response to stimuli of increasing frequency (all stimuli have a mean-to-peak amplitude of 1.5 μm, n = 24 cells in 18 flies).

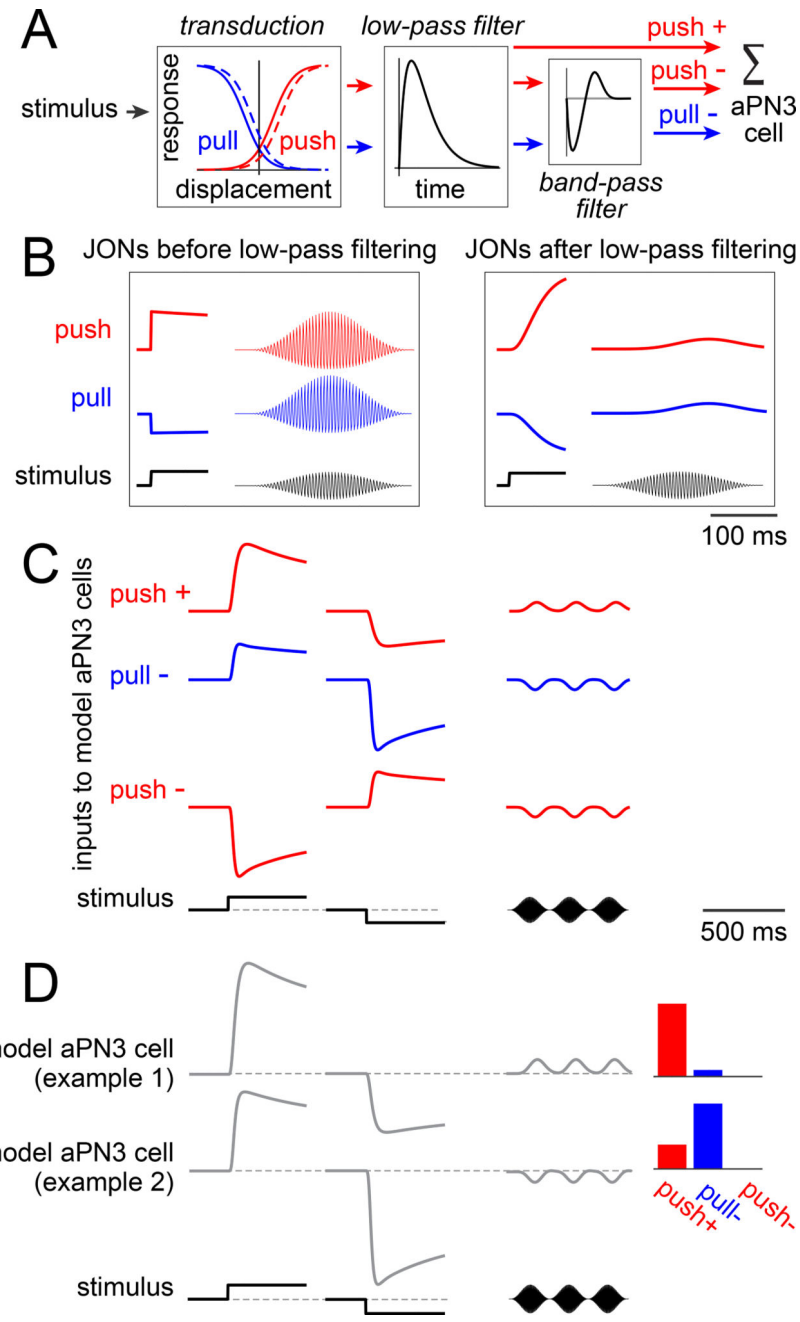

Figure 5. Linear combinations of peripheral inputs can account for many features of aPN3 neuron responses

A) Model components. Different model aPN3 neurons are generated by varying the weights on the three inputs to aPN3 neurons (push+, pull−, push−); all other parameters are fixed. B) Responses of model JONs before and after low-pass filtering. Shown here are responses to a sustained displacement and a 200 Hz sinusoid modulated at 4 Hz. Note that the push and pull JONs are anticorrelated in response to the sustained displacement, but positively correlated in response to sound. (Here, the pull channel has not yet passed through the bandpass filter, so the dynamics of the pull and push channels are still identical.)

C) The three inputs to model aPN3 neurons. Responses to three stimuli are shown here: a positive displacement of 2 μm, a negative displacement of 2 μm, and a sound stimulus (a 200 Hz sinusoid modulated at 4 Hz). The push+ and pull− inputs are positively correlated in response to a sustained displacement but negatively correlated in response to sound. Note that the time scale of this and the subsequent panel are compressed five-fold relative to (B). Adaptation in the excitatory input is due to the horizontal shift of the sigmoid curves; additional adaptation in the two inhibitory inputs are due to the bandpass filter.

D) Responses of two different model aPN3 neurons. These two models are illustrative examples because they combine the same two input channels (push+ and pull−) but with different weights. Bars at right represent the weights on the input channels. These model aPN3 neurons are positively correlated in response to a sustained displacement but negatively correlated in response to sound.

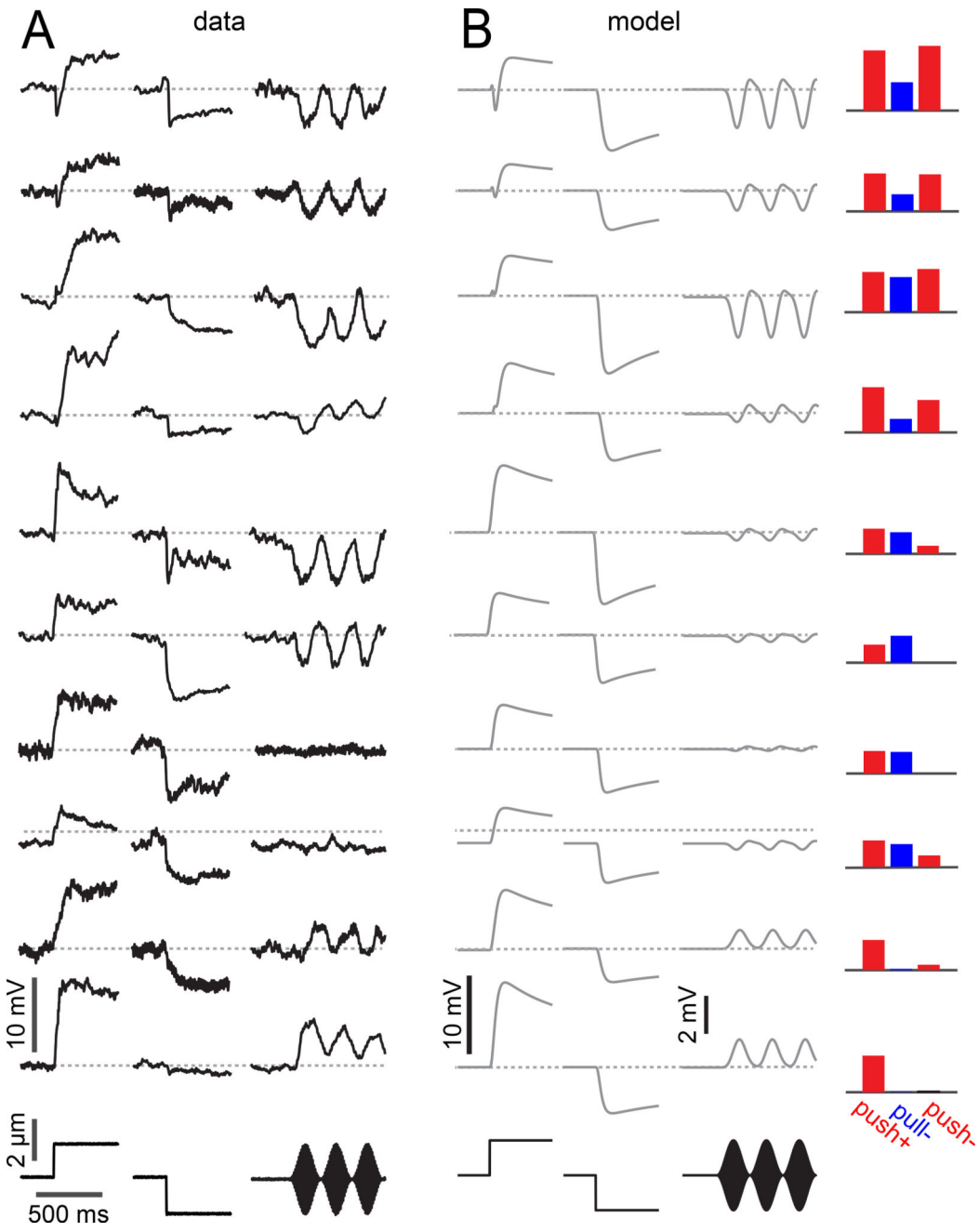

Figure 6. A simple model can capture most of the diversity in a population of aPN3 neurons

A) Average voltage in 10 example aPN3 neurons in response to three different stimuli (delivered with a piezoelectric device): sustained displacements of ±2 μm, plus a high frequency sound-like stimulus modulated at 4 Hz (carrier frequency 100 – 200 Hz). Notice that the step responses of these cells vary in their onset dynamics, and in the ratio of the positive step response to the negative step response. Similarly, sound responses vary in their sign, magnitude, and temporal dynamics. Cells also vary in the relative magnitude of their response to sound versus sustained displacements.

B) Modeled versions of the same 10 neurons (using the model in Figure 5). Model neurons differ only in the weights on their three inputs (push+, pull−, push−). Weights were constrained to be non-negative.

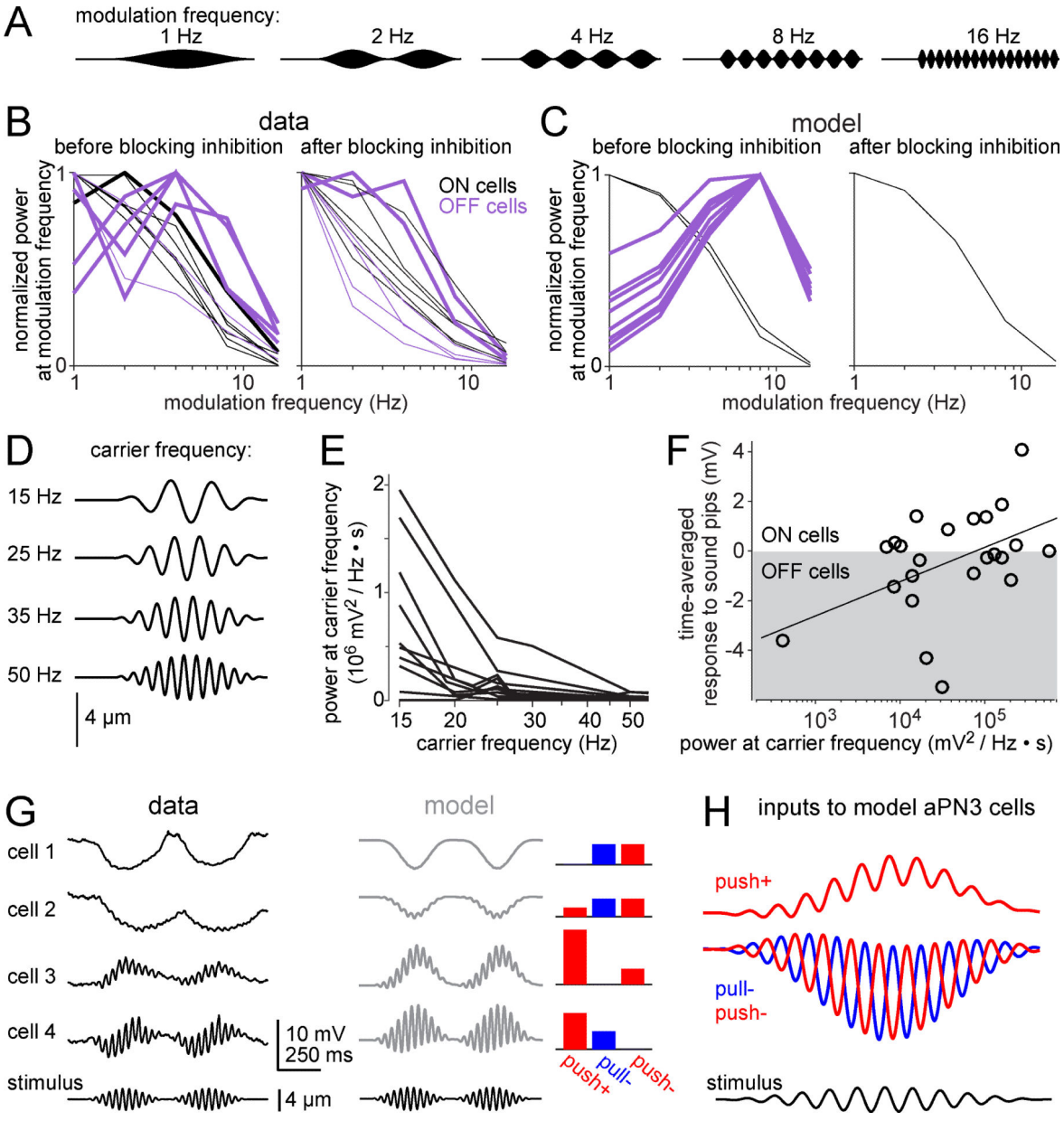

Figure 7. Different aPN3 neurons encode diverse temporal features of sound stimuli

A) A family of sound waveforms with a fixed carrier frequency (200 Hz) but different envelope frequencies (1 Hz to 16 Hz). Sounds were delivered via a speaker.

B) Envelope frequency tuning for 12 cells. ON cells in black, OFF cells in purple. Curves are normalized to each cell's peak. Thick lines are bandpass, thin lines are low-pass. Almost all curves are low-pass after blocking inhibition (using 5 µM picrotoxin with or without 50 µM CGP54626; see Experimental Procedures).

C) Envelope frequency tuning for the population of model neurons shown in Figure 6. Here, "blocking inhibition" involves setting inhibitory weights to zero, and it causes all model cells (ON and OFF) to have the same tuning.

D) Stimuli with a range of carrier frequencies, all modulated at an envelope frequency of 4 Hz. These stimuli were delivered using the piezoelectric actuator.

E) Power in the membrane potential at the stimulus frequency, for the stimuli in (D), measured in a population of aPN3 neurons (n = 24 cells; not all cells were stimulated with all frequencies).

F) Time-averaged voltage during the sound response versus power at the carrier frequency, for a 25 Hz carrier modulated at 4 Hz. Each symbol is a different cell (n = 23 cells in 17 flies). By definition, ON cells have a positive mean voltage and OFF cells have a negative mean voltage. There is a significant correlation between the mean voltage and log power at the carrier frequency ($R^2 = 0.28$, $p = 0.009$, two-tailed test of Pearson's correlation coefficient).

G) Left: Average voltage for four example aPN3 neurons in response to a fictive sound (25 Hz carrier modulated at 2 Hz). Some cells phase-lock to this carrier frequency, while others do not. Right: Modeled versions of the same neurons.

H) The three inputs to model aPN3 neurons (push+, pull−, push−), shown on an expanded time scale to display the phase relationships between different neurons. Here the stimulus is a 25 Hz carrier modulated at 2 Hz.

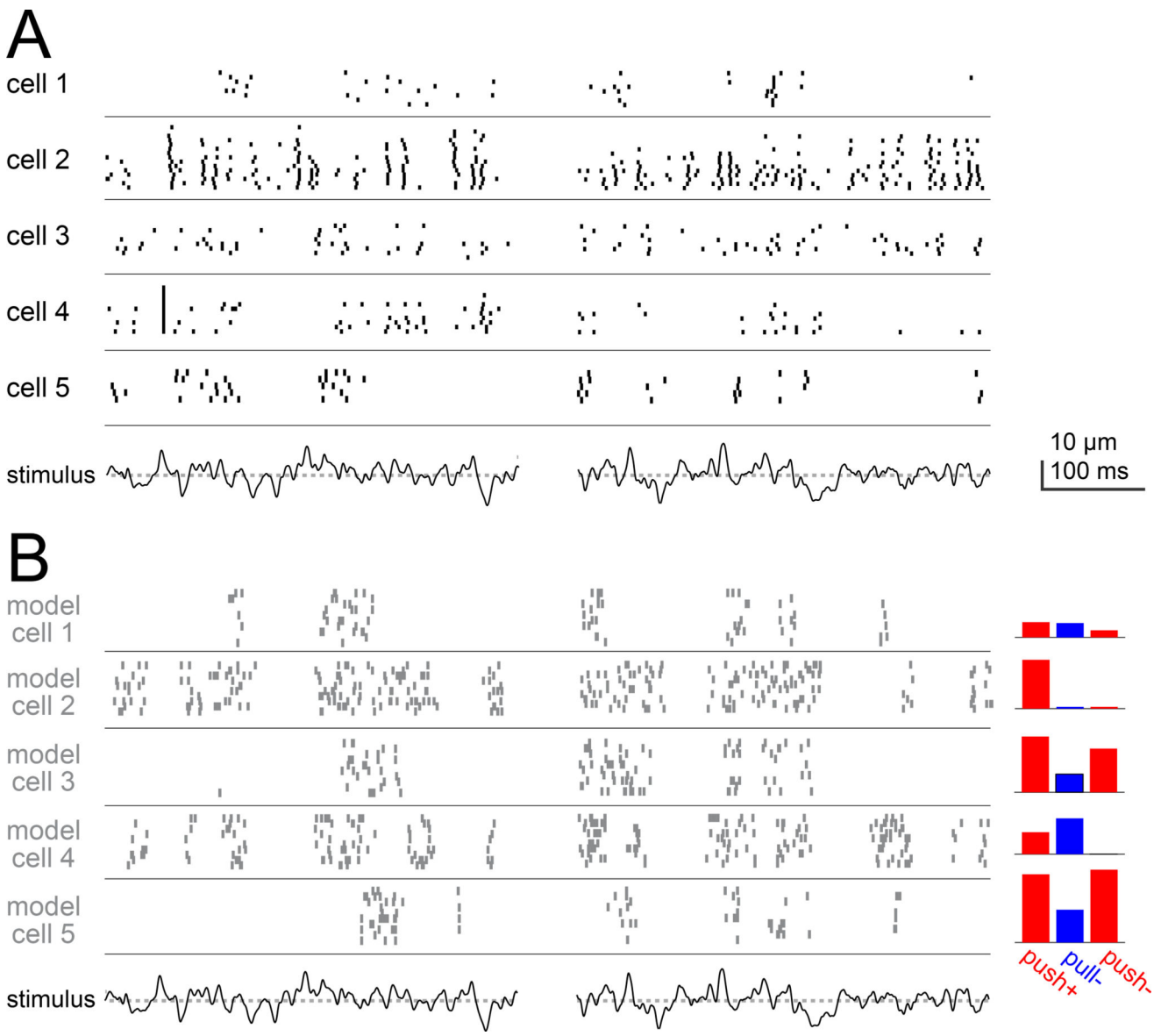

Figure 8. Different aPN3 neurons encode diverse temporal features of a wind-like stimulus

A) Spiking in six aPN3 neurons evoked by a ”wind”-like stimulus. The stimulus (bottom) was constructed so that its power spectrum emulates that of antennal movements evoked by wind (dotted line is zero displacement, i.e. the resting position of the antenna). Two snippets of this stimulus are shown.

B) Responses of six model aPN3 neurons to the same stimulus. This is a subset of the model cells in Figure 6, and their parameters were fit only to the data in Figure 6; they are not intended to match the individual cells in (A). Nonetheless, each of these cells is selective for different temporal features of the “wind”-like stimulus, and in this regard they resemble the cohort of cells in (A), which are also each selective for different temporal features. Here we explicitly model spikes, rather than simply modeling the aPN3 neuron membrane potential. The transformation from voltage to spikes in the model is given by a differentiating function,

in order to create the characteristic burstiness of aPN3 neurons (see Supplemental Experimental Procedures).